IS ELECTRON BEAM RADIATION SUITABLE FOR STERILIZATION OF MEDICAL PRODUCTS CONTAINING POLYETHYLENE TEREPHTHALATE GLYCOL?

Andrew Smith*, Md Kamrul Hasan†, and Leonard S. Fifield†

Pacific Northwest National Laboratory, Richland, WA, 99354

Abstract

Most medical products containing polyethylene terephthalate glycol (PETG) plastics are sterilized using either ethylene oxide gas or gamma radiation from the cobalt-60 radioisotope. Machine-based electron beam (e-beam) ionizing energy technology could be used to sterilize PETG-containing devices while avoiding perceived public health concerns and security risks associated with these current options. However, lack of available information regarding the effects of e-beam processing on plastics such as PETG remains a barrier for the medical device industry for broader e-beam use in sterilization. To support consideration of e-beam as a viable alternative for sterilization, this paper assesses changes in the carbonyl band in the IR spectrum, mechanical hardness and yellowness index of PETG tensile test strips at a series of sterilization-relevant doses: 15, 25, and 35 kGy. No significant changes were observed in the properties of the PETG materials evaluated at the e-beam doses considered.

†Corresponding authors: leo.fifield@pnnl.gov and kamrul.hasan@pnnl.gov *Undergraduate researcher and co-author
Keywords: E-beam, Polymers, Radiation, Sterilization, Color change, Hardness
Received: July 18, 2025 Accepted: July 25, 2025 Revision Received: September 16, 2025 Published: September 17, 2025

Introduction

Polyethylene terephthalate glycol (PETG) is a derivative of the common polyethylene terephthalate (PET) polymer, with an additional glycol modifier (**Figure 1**) that enhances strength and durability. Along with other biomedical and clinical medicine applications, the high impact resistance, durability, and formability of PETG make it one of the leading polymers used in medical device packaging.[1, 2] PETG-packaged medical devices are subject to sterilization to inactivate pathogens that may be present within each packaged product.

Ethylene oxide (EO) gas is used to sterilize half of the large number of single use medical devices produced globally, while four in ten products are sterilized using gamma radiation from the cobalt-60 radioisotope.[3] As the volume of medical devices produced each year continues to grow,[4] the capacity for EO sterilization faces capacity challenges, exacerbated by closures of facilities due to concerns for public safety.[5] Gamma radiation is effective in sterilizing PETG-containing products, but its use is challenged by the limited global sources of Co-60 and factors associated with its radioactive nature including safety, disposal, and activity decay.[6] Consequently, there is growing demand within the medical community to identify additional options for sterilization such as the machine-based ionizing energy sources of electron beam (e-beam) and X-ray. The energy output of accelerators used to produce e-beams can be tailored to balance penetration depth and throughput with electricity and shielding requirements to enable in-line or end-of-line sterilization of individual product units prior to secondary assembly and packaging in preparation for shipping.

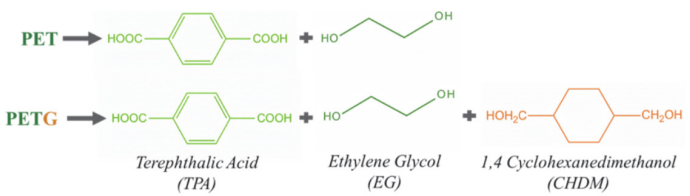

Figure 1. Monomer constitudents of PET and PETG.[19]

The high achievable dose rates of e-beam make such configurations attractive for sterilization of high volume products.[7] However, the effects of e-beam energy at sterilization-relevant doses on the plastics found in medical products in terms of biocompatibility, mechanical performance, and functionality are not well known.[8, 9]

In response to ionizing radiation, polymers undergo oxidation, chain scission, and/or cross-linking, depending on the inherent susceptibilities in the polymeric backbones and the irradiation conditions.[10] Cross-linking forms molecular networks, increasing polymer strength, but can lead to embrittlement. Chain scission involves random bond rupturing, reducing polymer strength.[7] Physical changes to materials from ionizing energy can also entail discoloration, stiffening, and softening from alterations in chemical structure. Changes due to sterilization processing of a polymer-containing device must be acceptable for the safety and function of the product. Sterilization ionizing radiation doses are typically 15-50 kGy, establised by bioburden-based validation methods.[11,12] In previous studies, irradiated PET exhibits lowered intrinsic viscosity (IV) and molecular weight, indicating chain scission as the main reaction.[13, 42] Adsorbed e-beam dose up to 150 kGy did not induce new functional groups in PET. However, increased doses led to a slight rise in crystallinity, attributed to chain scission and rearrangement into crystalline structures, which also reduced permeability.[15] Gamma radiation, which has a higher penetration ability than e-beam, minimally affects the physicochemical properties of PET packaging film up to the dose of 200 kGy.[16] At higher doses, particularly above 2000 kGy, the mechanical properties of PET deteriorate, with reduced tensile elongation at break (EAB) due to material degradation and increased carbonization.[17] 3D-printed PETG parts exposed to gamma doses of 0.75, 1.5, and 2.25 MGy, revealed decreased ultimate tensile stress and decreased EAB.[18] Prior reported studies on the effects of radiation on PETG are either limited to PET material or to 3D-printed materials or gamma irradiation at a dose levels beyond sterilization applications.

This paper examined material parameters such as changes in the yellowness index as a measure of color change, carbonyl index

as a measure of oxidation, and mechanical hardness of PETG as indicators of material integrity following e-beam processing to 15, 25, and 35 kGy dose levels. We hypothesize that the measured material property effects of e-beam processing at these sterilization-relevant doses will not preclude the use of e-beam for sterilization of PETG-containing products.

Experimental Methods

Evaluated Materials

The two grades of PETG materials evaluated in this study, referred to as PETG-1 and PETG-2, were supplied directly from Terumo Blood and Cell Technologies (Terumo BCT, Inc.) and represent formulations used in the Rika plasma donation and Trima automated blood collection devices, respectively. The materials were provided as 3.25-mm thick, 214-mm long dumbbell-shaped specimens, as shown in **Figure 2**.

E-beam Processing

PETG specimens were irradiated at E-beam Services, Inc. (Cranbury, NJ) using a 4.0 MeV scanned electron beam to target absorbed doses of 15, 25, and 35 kGy. Irradiations were performed in ambient air at room temperature and facility ambient humidity. The accelerator operated in scanned-beam mode with a magnetic sweep across the product width; the beam was not focused on a spot. Uniformity and delivered dose were controlled by adjusting scan width and frequency, beam current, and conveyor speed. Pre-run and in-process dose mapping verified spatial uniformity across the coupon face. Calibrated B3 radiochromic film dosimeters were placed on the top and bottom surfaces of representative specimens at center and near-edge locations to determine the minimum absorbed dose (D_{min}), maximum absorbed dose (D_{max}), and the dose-uniformity ratio, DUR ($DUR = D_{max}/D_{min}$). These dosimetry and process-control measures confirmed the actual absorbed doses for all conditions.

Yellowness Index (YI) Measurement

To quantify visual changes with exposure to e-beam, the yellowness index (YI) of the polymers was assessed following the ASTM E313 standard. The measurement utilized established methods[9, 20, 21] employing a Nikon D5300 digital camera and a GTI MiniMatcher MM 2e light booth. Under D65 lighting conditions within the light booth, digital images of specimens for each exposure condition were captured. Subsequently, the collected images were analyzed using ImageJ software to convert colors into absolute measures (XYZ color space). YI calculations were performed by selecting regions of interest (ROI), obtaining XYZ color space values, and adhering to calculation guidelines outlined in ASTM E313. The YI was calculated following the equation below.

$$YI = 100(C_xX - C_zZ)/Y$$

For each exposure condition, five replicate specimens were evaluated; for each specimen, three images were acquired, and a ROI was selected on each image. The test setup is shown in **Figure 3**.

Fourier transform infrared spectroscopy (FTIR) and Carbonyl Index (CI) Measurement

FTIR serves as a tool for identifying chemical alterations in materials by monitoring absorption intensities at specific absorbance energies. This method facilitates the determination of the carbonyl index (CI), which follows the transformation of C-C or C-H bonds into carbonyl (C=O) bonds due to oxidation.[22] In this study, CI was assessed to monitor oxidation induced by e-beam processing. FTIR analysis was conducted using a Bruker Alpha II OPUS Touch spectrometer equipped with an attenuated total reflection (ATR) accessory. Specimens were positioned centered on a diamond ATR crystal, and 64 scans were accumulated between 4000 and 400 cm^{-1} at a resolution of 4 cm^{-1} to minimize signal fluctuations attributable to noise. To mitigate measurement bias, three readings were taken per specimen. The carbonyl index was calculated as the ratio between the absorbance intensity of the carbonyl peak (at 1712 cm^{-1} for PETG-1 and 1715 cm^{-1} for PETG-2) and that of the methylene symmetric stretch peak (the highest point between 2850 and 2846 cm^{-1}) following the equation below.

$$CI = \frac{C = O_{peak}}{C - H_{peak}}$$

Hardness (H) Measurement

The hardness of the materials was determined on the Shore M scale using a durometer. All samples were preconditioned for at least 40 hours at 23 ± 2 °C, 50 ± 10% relative humidity (following ASTM D618-13), and tests were performed in a controlled environment (following ASTM D2240-15) using a Rex Model DD-4 Type M Digital Durometer with a pneumatically damped Model OS-1 Operating Stand (Rex Gauge Company, Inc.). Three measurements were performed on each specimen with a minimal distance of 0.80 mm between each tested location on the sample to account for variance from nominal readings. A digital image of the durometer used to perform these tests can be seen in **Figure 4**.

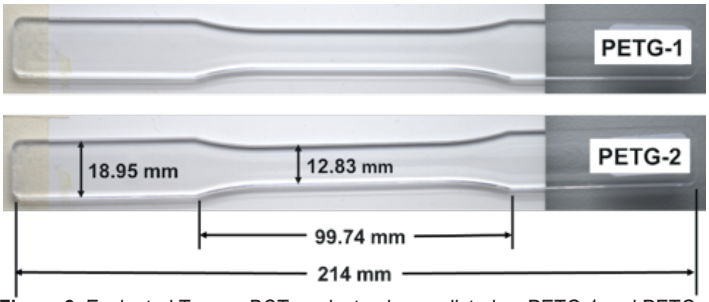

Figure 2. Evaluated Terumo BCT product polymers listed as PETG-1 and PETG-2.

Figure 3. Yellowness index color test setup

Elongation at Break (EAB) and Tensile Strength (TS) Measurement

Uniaxial tensile tests were performed in accordance with ASTM D638 after completion of hardness measurements. Dumbbell specimens were marked at the center of the gauge section with a permanent marker to define the initial gauge length of 55 mm, then carefully centered and aligned in an Instron 3367 universal testing machine equipped with pneumatic grips. The crosshead speed (50 mm/min for PETG-1) was set according to ASTM D638 guidelines to achieve failure within 30 seconds to 5 minutes. Tests were conducted under laboratory ambient conditions. Each test was video-recorded (Nikon D7500) and analyzed with a computer-vision video-extensometry workflow (https://github.com/pnnl/maadsci-extensometry) to obtain elongation at break (EAB) and tensile strength (TS).

Statistical analysis

Statistical analysis was performed to evaluate the effects of e-beam dose on the material properties at three doses of 15, 25, and 35 kGy using R software (R Core Team, 2019) with a significance level of $p \leq 0.05$ and a confidence interval of 95%. A larger p-value suggests that changes in the e-beam dose are not associated with changes in the property explored (insignificant).

Results

A comparison between material PETG-1 and material PETG-2 at the 4.0 MeV energy level was sought to examine the material properties across various doses (15, 25, and 35 kGy). Commercial e-beam sterilization facilities commonly operate at 10 MeV, but lower energy e-beam options are of growing interest for smaller footprint accelerators, such as for use in-line or at end-of-line versus following packaging in the device manufacturing process. Focusing on the dose effects yielded insights into the potential ramifications of e-beam irradiation on the physical attributes of PETG polymers.

Yellowness Index (YI)

The yellowness index of both PETG-1 and PETG-2 increased with e-beam dose beyond the standard deviation of the unirradiated samples, as shown in **Figure 5**. The differences from the unirradiated samples are most noticeable at the highest dose of 35 kGy (~3.63% increase on average for PETG-1 and ~5.78% on average for PETG-2). However, when comparing the effects among e-beam doses (15, 25, 35 kGy), the statistical analysis detected a significant increase of YI only for PETG-1 (p-value of 0.007), whereas no significant change was observed for PETG-2. Photos of the materials at different doses are captured in **Figure 6**. Visual properties and color change of medical devices following sterilization are important considerations for end users.

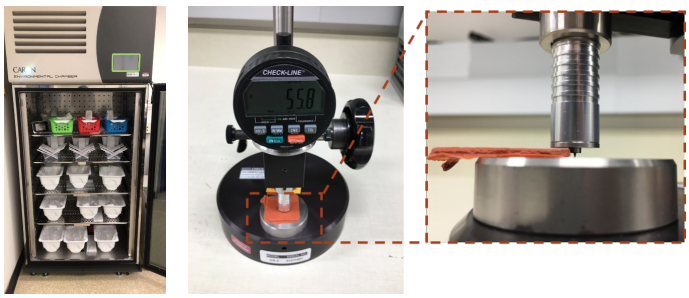

Figure 4. Sample conditioning in the environmental chamber (left image) and Shore M durometer for hardness tests (right image).

Fourier transform infrared spectroscopy (FTIR) and Carbonyl Index (CI)

Material identity was confirmed through FTIR spectra before and after e-beam exposure. In both cases, materials had identifiable peaks corresponding to chemical bonds in PETG, as seen in **Table 1** and **Figures 7-11**. **Figure 7** shows the FTIR spectra of PETG-1 and PETG-2, in which the peaks at 2926 and 2854 cm^{-1} are attributed to the C-H asymmetric and symmetric aliphatic stretching vibrations in the polymeric chains.[23] The intense peak at 1712 cm^{-1} indicates the C=O of ester groups, and the C–H out-of-plane deformation of two carbonyl substituents on the aromatic ring is observed at 730 cm^{-1}.[22, 24] The two peaks at 1450 and 1259 cm^{-1} are attributed to the C-H bending of the methylene group and

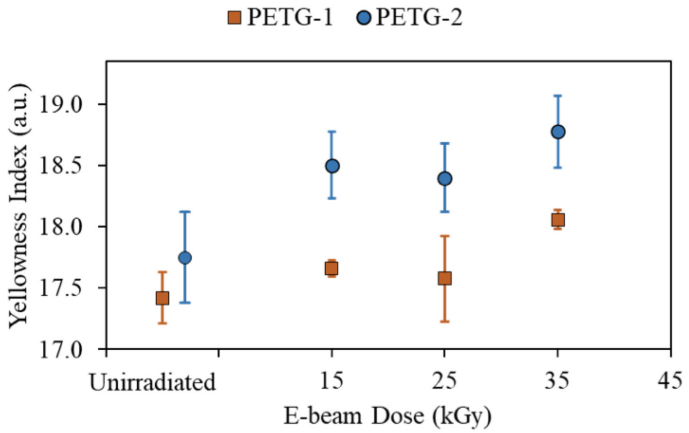

Figure 5. Graph displaying the average yellowness index of PETG-1 and PETG-2 materials at 15, 25, and 35 kGy dose levels and their respective unirradiated materials.

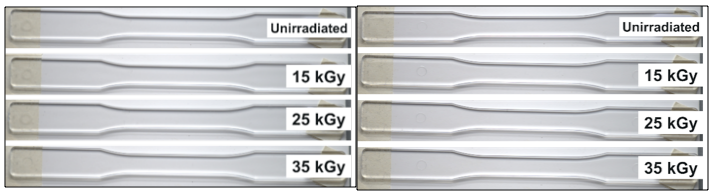

Figure 6. PETG-1 (left image) and PETG-2 (right image) materials at 15, 25, and 35 kGy dose levels and their respective unirradiated materials.

Table 1. PETG-1 significant FTIR peaks and corresponding chemical bonds.

Wavenumbers Obtained (cm^{-1})	Assignment[22-26]
2926 (PETG-1); 2932 (PETG-2)	C-H asymmetric stretching
2854	C-H symmetric stretching
~2350	Atmospheric CO_2
1712 (PETG-1); 1715 (PETG-2)	C=O stretching of ester groups
1450	C-H bending of methylene group
1259	C-O stretching of ester groups
1098	C–O stretching
1018	C–H bonds in-plane vibrations
956	C–H stretching of cyclohexene ring
876, 725	C–H out-of-plane deformation of two carbonyl substituents on the aromatic ring

the C–O stretching of the ester groups, respectively.

As shown in **Figure 7**, the peaks in PETG-2 exhibit a drop in absorbance in the overall spectrum compared to PETG-1. This may be due to the differences in contact status between the two measurements. The contact pressure applied might be higher towards PETG-1 as it is softer compared to PETG-2 (see **Figure 13**). Around 2350 cm^{-1} wavenumber, a broad, rounded double peak is observed, indicating the presence of atmospheric carbon dioxide and might be an artifact of the measurement.

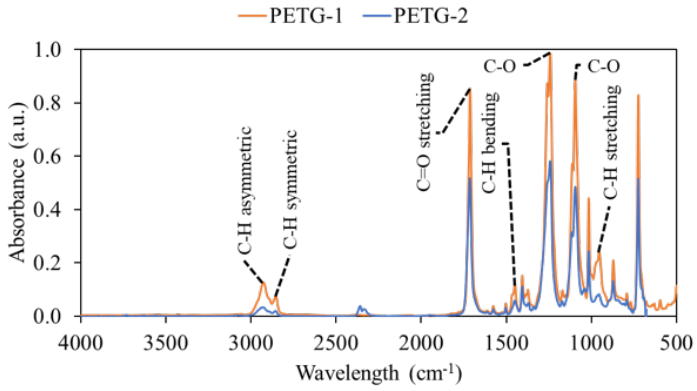

Figure 7. FTIR spectra for unirradiated control samples with PETG signaling peaks identified.

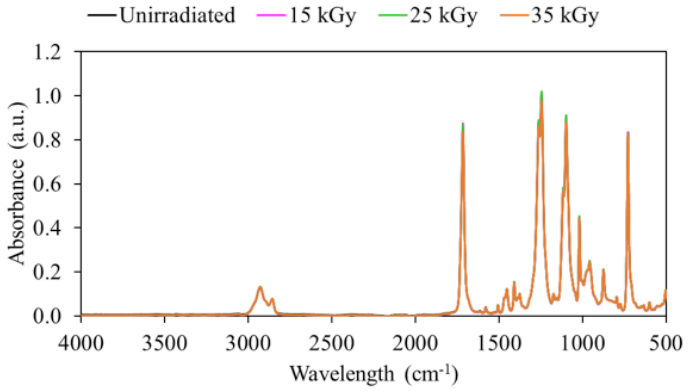

Figure 8. FTIR Spectra for PETG-1 at 15, 25, and 35 kGy at the 4 MeV energy level along with the unirradiated PETG-1.

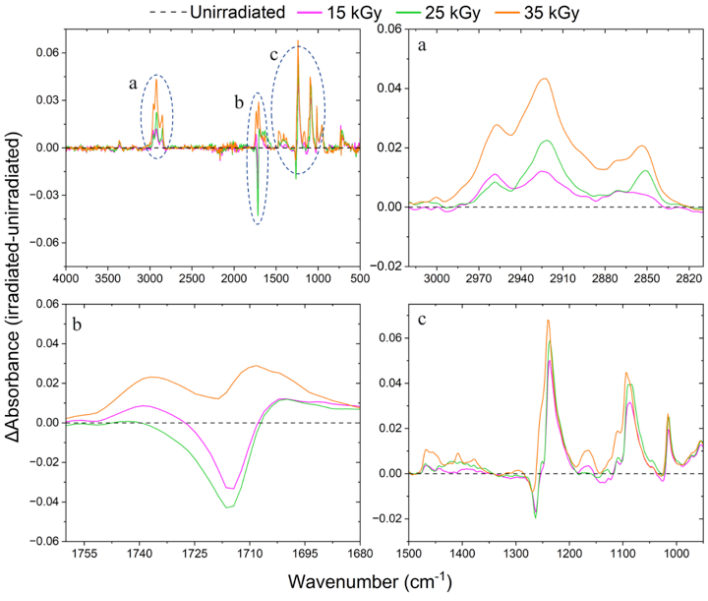

Figure 9. FTIR difference spectra ($\Delta A = A_{irradiated} - A_{unirradiated}$) for PETG-2 at 15, 25, and 35 kGy. The black dashed line denotes the unirradiated reference ($\Delta A = 0$). Left: full spectrum; right panels (a–c) zoom the CH-stretch region (3020–2810 cm^{-1}), the ester carbonyl band (1760–1680 cm^{-1}), and the fingerprint region (1500–950 cm^{-1}).

FTIR difference spectra (ΔAbsorbance, defined as $\Delta A = A_{irradiated} - A_{unirradiated}$) in Figure 9 for PETG-1, at 15, 25, and 35 kGy, remain close to zero across the full range after baseline correction, normalization to the 870 cm^{-1} peak, and averaging n=3 replicates. Only small, dose-ordered residuals are observed at native PETG bands, most prominently within the C–H stretching envelope (≈3020–2810 cm^{-1}) and at selected fingerprint features (≈1500–950 cm^{-1}). These features are modest in magnitude (generally a few 10^{-3}–10^{-2} absorbance units, ≤ ~0.06 at the most intense feature) and do not introduce new absorptions. The ester carbonyl band (≈1712 cm^{-1}) shows a narrow negative lobe but no monotonic increase with dose, indicating no detectable oxidation under the conditions studied.

PETG-2 exhibits the same qualitative response in **Figure**

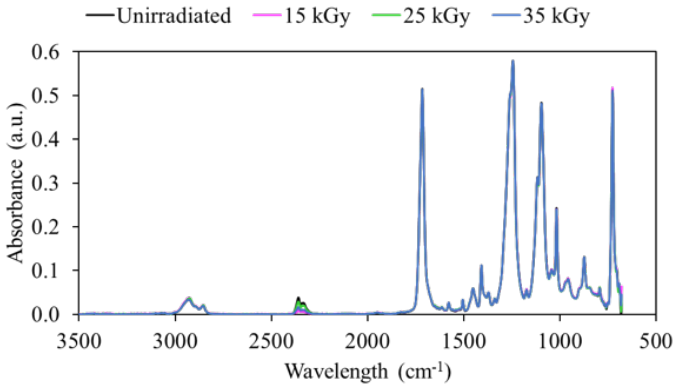

Figure 10. FTIR spectra for PETG-2 at 15, 25, and 35 kGy at the 4 MeV energy level along with the unirradiated PETG-2.

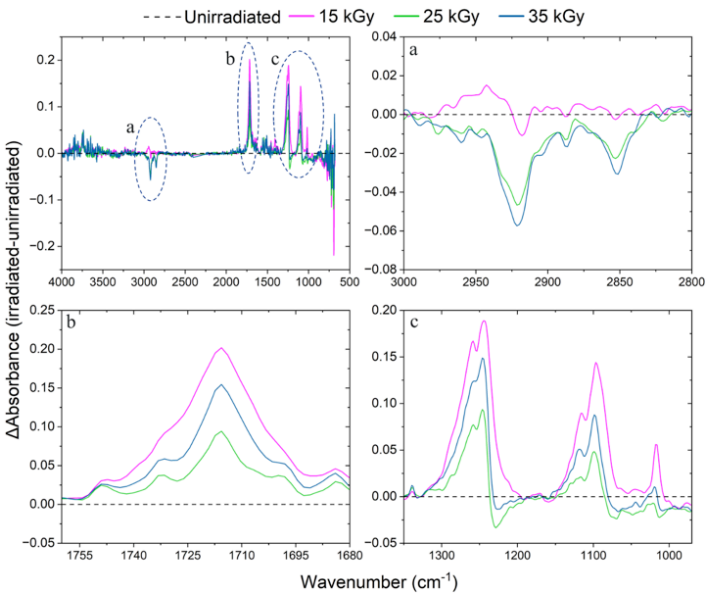

Figure 11. FTIR difference spectra ($\Delta A = A_{irradiated} - A_{unirradiated}$) for PETG-2 at 15, 25, and 35 kGy. The black dashed line denotes the unirradiated reference ($\Delta A = 0$). Left: full spectrum; right panels (a–c) zoom the CH-stretch (3000–2800 cm^{-1}), ester C=O (1760–1680 cm^{-1}), and fingerprint (~1350–970 cm^{-1}) regions.

11. ΔA traces lie near zero and all residuals coincide with existing PETG bands. Slightly larger excursions appear in the C–H stretching region (≈3000–2800 cm^{-1}) and around strong fingerprint modes (≈1350–970 cm^{-1}, especially near 1100–1000 cm^{-1}), with amplitudes greatest at 35 kGy yet non-monotonic overall. As with PETG-1, the carbonyl index (see **Figure 12**) remained almost identical to the unirradiated samples across all three doses, indicating no increase in oxidation during irradiation, and no new absorptions were observed. Taken together, the two materials show no dose-dependent emergence of new functionality and no systematic carbonyl growth, supporting that e-beam sterilization at 15–35 kGy does not measurably alter the FTIR-detectable chemistry of these PETG formulations. Residual differences are consistent with minor normalization/ATR-contact or packing effects rather than radiation-induced chemical change.

Hardness (H)

Figure 13 shows the changes in Shore M hardness values on the PETG materials with e-beam dose. Both PETG materials experienced a marginal decrease in hardness value with dose level in similar fashion. Still, the reduction of hardness fell within the sensitivity limits of the measurement and is therefore considered statistically insignificant to e-beam irradiation doses up to ~ 35 kGy.

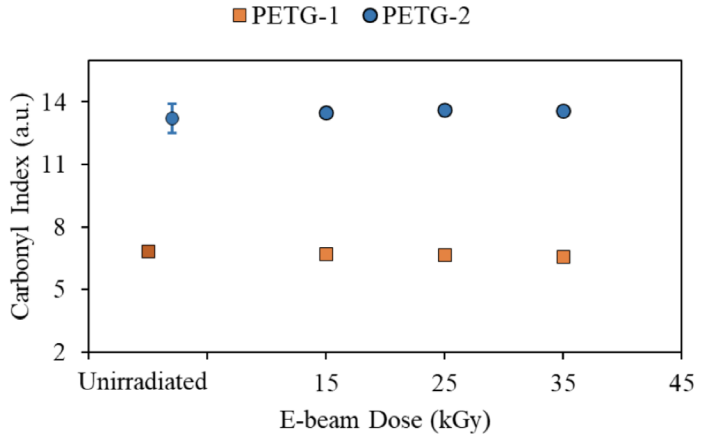

Figure 12. Graph displaying the average carbonyl index of PETG-1 and PETG-2 materials at 15, 25, and 35 kGy dose levels and their respective unirradiated materials.

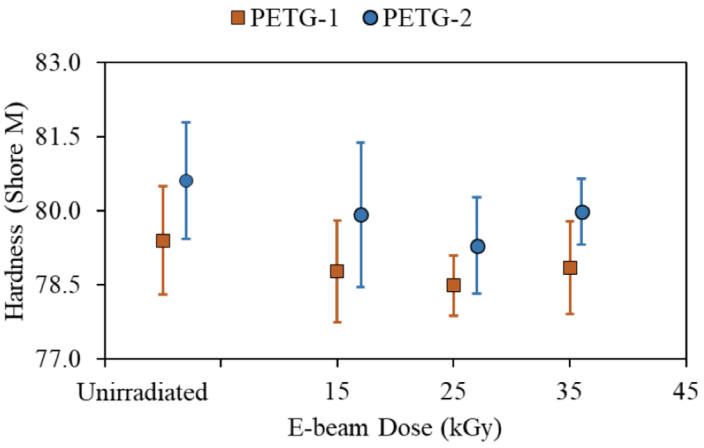

Figure 13. Graph displaying the average hardness level of PETG-1 and PETG-2 materials at 15, 25, and 35 kGy dose levels and their respective unirradiated materials. PETG−2 points have been offset along the x−axis for clarity of their error bars.

Discussion

To assess the viability of mid-energy e-beam sterilization of medical devices, an investigation into its impact on the physical characteristics of polymers was conducted. This paper focuses on two materials, both PETG, subjected to varying doses of e-beam exposure (15, 25, 35 kGy) at 4.0 MeV energy, followed by a comprehensive physical analysis. The trend of yellowness index for PETG-1 is observed to be positively correlated with increasing dose, whereas the hardness of that material is negatively correlated with dose. Notably, the increase in the YI was above the control values, and statistically detectable differences were observed with dose only for PETG-1. Although a slight increase in YI was measured, it does not affect sterility or device performance, and shifts were generally below visual detectability. In contrast, the carbonyl index remained relatively unchanged across all doses, supporting the insignificance of oxidation reactions for the conditions explored. The hardness values with dose fell within the standard deviation of the control and, therefore, are considered insignificant. The close alignment of average values with standard deviation for tensile property tests (elongation at break and tensile strength) of PETG material sourced from the two materials suggests that e-beam sterilization adequately meets the structural integrity (see **Figure 14** for PETG-1**)**. A comparative analysis between material PETG-1 and material PETG-2 revealed consistent trends, with slightly elevated values for the first. Both materials demonstrated stability in their respective properties throughout the experimentation. The changes in the investigated properties due to e-beam irradiation can be summarized in **Table 2**. Overall, within 15–35 kGy, e-beam sterilization did not measurably alter FTIR-detect-

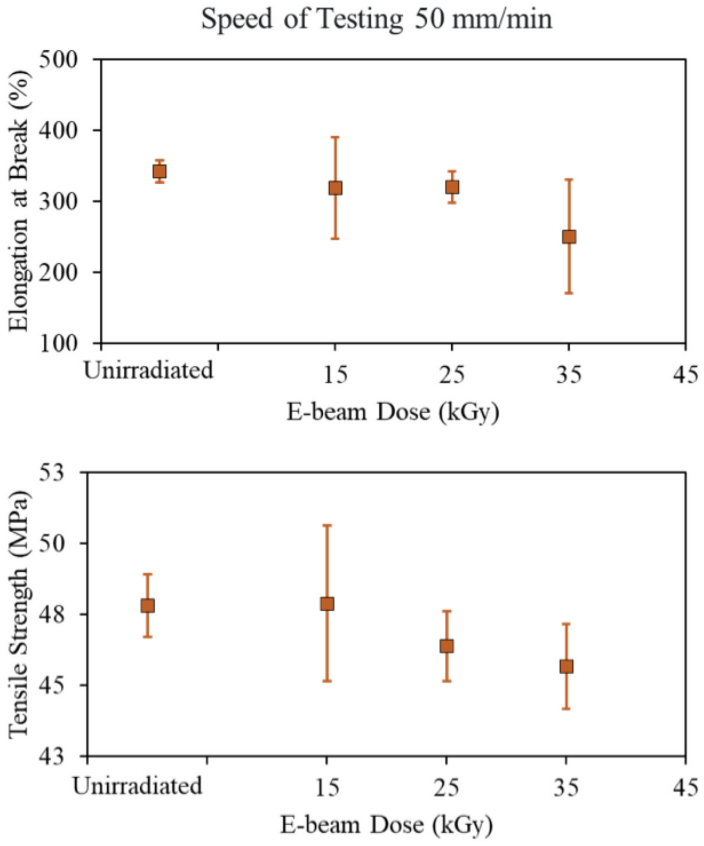

Figure 14. Graph displaying the average elongation at break (top image) and tensile strength (bottom image) of PETG-1 material at 15, 25, and 35 kGy dose levels and their respective unirradiated materials.

able chemistry or mechanical performance, and any color change was small and typically imperceptible to the unaided eye.

These results have practical implications for the community. They de-risk PETG for use with compact, lower-energy e-beam accelerators suitable for in-line or end-of-line sterilization, offering an alternative to EO and Co-60 gamma that can enhance supply-chain resilience, safety, and logistics. Because the studied dose window (15–35 kGy) lies within ISO 11137 bioburden-based ranges, the data can streamline regulatory bridging from gamma to e-beam for PETG components, with additional testing focused on device-specific materials (e.g., adhesives, inks, elastomers). In practice, dose mapping, scan-parameter control, and management of dose-uniformity ratio (D_{max}/D_{min}) provide a clear implementation path for typical PETG packaging and fluid-path geometries; appearance can be maintained via simple color specifications and, if needed, anti-yellowing stabilizers. Limitations include penetration depth and shadowing at 4 MeV and the need to extend compatibility evidence to additional polymers, multi-material assemblies, shelf-life, and full biocompatibility. Taken together, the findings support safe, decentralized adoption of low-energy e-beam as a viable sterilization option for PETG-containing medical products.

Conclusion

The results from this study reinforce our hypothesis of e-beam ionizing energy as a viable sterilization source for the investigated PETG polymers based on the effects of processing on material exposure. At sterilization-relevant doses, e-beam effects on the measured properties of the two PETG polymers were only found to be statistically significant in the case of yellowing for PETG-1. An FTIR analysis of polymer oxidation via consideration of carbonyl index showed equivalent values for samples before and after e-beam processing. Although trends with dose were observable for hardness values of the two plastics, they fell within the standard deviation range of the material measurements. Yellowness index rose with increasing dose, making it statistically notable for PETG-1. However, the detected significance of yellowing in PETG-1 does not necessarily mean that e-beam is not a suitable device sterilization option. Detectable differences were small in absolute terms, and it is up to the manufacturer to determine if the yellowing is acceptable for their commercial product. Overall, these data support e-beam as a viable ionizing energy source for sterilizing products containing PETG.

Acknowledgments

The authors would like to thank Ilya Getser and Terumo BCT, Inc. for providing the product materials for this research, Gustavo Varca and E-beam Services Inc. for irradiating the products with E-beam, and Mark Murphy and Jen Elster at Pacific Northwest National Laboratory (PNNL) for providing leadership on this project. The authors also acknowledge Angel Ortiz for performing the hardness test, Yelin Ni for the yellowness index measurement, and Donghui Li for the FTIR measurement. This work was supported by the U.S. Department of Energy National Nuclear Security Administration Office of Radiological Security. PNNL is operated by Battelle for the U.S. Department of Energy under Contract DE-AC05-76RL01830

Table 2. Summary of observed statistically detectable differences due to e-beam doses

Material	CI	YI	H	EAB	TS
PETG-1	NS	*Increase with dose*	NS	NS	NS
PETG-2	NS	NS	NS	NS	NS

CI = carbonyl index; YI = yellowness index; H = hardness; EAB = elongation at break; TS = tensile strength; NS = not significant

References

1. Yan, C.; Kleiner, C.; Tabigue, A.; Shah, V.; Sacks, G.; Shah, D.; DeStefano, V. PETG: *Engineered Regeneration* **2024**, *5* (1), 45-55. DOI: https://doi.org/10.1016/j.engreg.2023.11.001.
2. Durga Rajesh, K. V.; Ganesh, N.; Yaswanth Kalyan Reddy, S.; Mishra, H.; Teja Naidu, T. M. V. P. S. *Materials Today: Proceedings* **2023**. DOI:https://doi.org/10.1016/j.matpr.2023.06.343
3. Alliance, G. I. P.; Association, I. I. A comparison of gamma, E-beam, X-ray and ethylene oxide technologies for the industrial sterilization of medical devices and healthcare products. 2017.
4. Pandey, D. *Medical Disposables Market Size, Share, and Trends 2025 to 2034*; Report Code 1014; Precedence Research, January 2025. https://www.precedenceresearch.com/medical-disposables-market (accessed 22 February 2025).
5. Rutala, W. A.; Weber, D. J. *American Journal of Infection Control* **2023**, *51* (11, Supplement), A82-A95. DOI: https://doi.org/10.1016/j.ajic.2023.01.020.
6. Kroc, T. K.; Thangaraj, J. C.; Penning, R. T.; Kephart, R. D. *Accelerator-driven medical sterilization to replace Co-60 sources*; Fermi National Accelerator Lab.(FNAL), Batavia, IL (United States), 2017.
7. Hasan, M. K.; Staack, D.; Pillai, S. D.; Fifield, L. S.; Pharr, M. C., *Polymer Degradation and Stability* **2024**, *221*, 110677. DOI: https://doi.org/10.1016/j.polymdegradstab.2024.110677.
8. Fifield, L. S.; Pharr, M.; Staack, D.; Pillai, S. D.; Nichols, L.; McCoy, J.; Faucette, T.; Bisel, T. T.; Huang, M.; Hasan, M. K.; et al. *Radiation Physics and Chemistry* **2021**, *180*, 109282. DOI: https://doi.org/10.1016/j.radphyschem.2020.109282.
9. Fifield, L. S.; Pharr, M.; Staack, D.; Pillai, S. D.; Nichols, L.; McCoy, J.; Faucette, T.; Bisel, T. T.; Huang, M.; Hasan, M. K.; et al. *Radiation Physics and Chemistry* **2021**, *186*, 109505. DOI: https://doi.org/10.1016/j.radphyschem.2021.109505.
10. Spadaro, G.; Alessi, S.; Dispenza, C. *Applications of ionizing radiation in materials processing* **2017**, *1*, 167-182.
11. ISO, D. Sterilization of Health Care Products–Radiation–Part 2: Establishing the Sterilization Dose. ISO 11137-2: 2012 2013.
12. TIR17, A. Compatibility of materials subject to sterilization. Arlington, VA: Association for the Advancement of Medical Instrumentation 2017.
13. Chikaoui, K. *Radiation Physics and Chemistry* **2019**, *162*, 18-22. DOI: https://doi.org/10.1016/j.radphyschem.2019.04.034.
14. Buttafava, A.; Consolati, G.; Di Landro, L.; Mariani, M. *Polymer* **2002**, *43* (26), 7477-7481. DOI: https://doi.org/10.1016/S0032-3861(02)00708-5.
15. Caire-Maurisier, F.; Aymes-Chodur, C.; Jandard, V.; Bourrel, A.; Yagoubi, N. *Annales Pharmaceutiques Françaises* **2019**, *77* (4), 276-285. DOI:https://doi.org/10.1016/j.pharma.2019.02.001.
16. Jeon, D. H.; Lee, K. H.; Park, H. J. *Radiation Physics and Chemistry* **2004**, *71* (5), 1059-1064. DOI: https://doi.

org/10.1016/j.radphyschem.2003.10.009.
17. Jamalzadeh, M.; Sobkowicz, M. J. *Polymer Degradation and Stability* **2022**, *206*, 110191. DOI: https://doi.org/10.1016/j.polymdegradstab.2022.110191.
18. Cressall, S.; Phillips, C. O.; Al-Shatty, W.; Deganello, D. *Journal of Materials Science* **2024**, *59* (4), 1768-1782. DOI: 10.1007/s10853-023-09309-2.
19. Sastri, V. R. 6 - Engineering Thermoplastics: Acrylics, Polycarbonates, Polyurethanes, Polyacetals, Polyesters, and Polyamides. In Plastics in Medical Devices (Third Edition), Sastri, V. R. Ed.; William Andrew Publishing, 2022; pp 167-232.
20. Li, D.; Bisel, T. T.; Cooley, S. K.; Murphy, M. K.; Spencer, M. P.; Hasan, M. K.; Fifield, L. S.; Pharr, M.; Staack, D.; Huang, M.; et al. *Radiation Physics and Chemistry* **2024**, *223*, 111971. DOI: https://doi.org/10.1016/j.radphyschem.2024.111971.
21. Li, D.; Bisel, T. T.; Cooley, S. K.; Ni, Y.; Murphy, M. K.; Spencer, M. P.; Hasan, M. K.; Fifield, L. S.; Pharr, M.; Staack, D.; et al. *Radiation Physics and Chemistry* **2025**, *226*, 112188. DOI: https://doi.org/10.1016/j.radphyschem.2024.112188.
22. Paszkiewicz, S.; Szymczyk, A.; Pawlikowska, D.; Irska, I.; Taraghi, I.; Pilawka, R.; Gu, J.; Li, X.; Tu, Y.; Piesowicz, E. S. *RSC advances* **2017**, *7* (66), 41745-41754.
23. Chen, T.; Zhang, J.; You, H. *RSC Advances* **2016**, *6* (104), 102778-102790, 10.1039/C6RA21985C. DOI: 10.1039/C6RA21985C.
24. Chen, T.; Zhang, W.; Zhang, J. *Polymer Degradation and Stability* **2015**, *120*, 232-243. DOI: https://doi.org/10.1016/j.polymdegradstab.2015.07.008.
25. Latko-Durałek, P.; Dydek, K.; Boczkowska, A. *Journal of Polymers and the Environment* **2019**, *27* (11), 2600-2606. DOI: 10.1007/s10924-019-01544-6.
26. Xiang, B.; Wang, X.; Wu, G.; Xu, Y.; Wang, M.; Yang, Y.; Wang, Q.*Scientific Reports* **2021**, *11* (1), 10052. DOI: 10.1038/s41598-021-89425-8.